Journal of Research and Applications in Mechanical Engineering
ISSN: 2229-2152 (Print); 2697-424x (Online)
(2024) Vol. 12, No. 1, Paper No. JRAME-24-12-006
[DOI: 10.14456/jrame.2024.6]

*Research Article*

# Parametric Study on Water-Cooling Plates to Improve Cooling Performance on 18650 Li-ion Battery

**R. Nanthatanti**[1]
**J. Charoensuk**[1,*]
**M. Masomtob**[2]
**S. Hirai**[3]
[1]*Department of Mechanical Engineering, Faculty of Engineering, King Mongkut's Institute of Technology Ladkrabang, Bangkok 10520, Thailand*
[2]*Energy Innovation Research Group (EIRG), National Energy Technology Centre (ENTEC), National Science and Technology Development Agency (NSTDA), Pathum Thani 12120, Thailand*
[3]*Department of Mechanical Engineering, Tokyo Institute of Technology, Tokyo, Japan*

**Received** 27 April 2023
**Revised** 13 July 2023
**Accepted** 24 August 2023

**Abstract:**
*With a novel NSTDA design, pressure drop, and standard deviation of cooling water velocity inside the channel of the liquid cooling plate were evaluated under various channel counts [2, 3, 4, and 6 channels per base], inlet temperatures of water [25, 30, 35, and 40 °C], and inlet velocity of water [0.5, 1.0, 2.0, and 3.0 m/s] at steady-state conditions. It was found that the 4-channel design produced the most distributed flow with an inlet water velocity of 0.5 m/s. The average channel velocity was 0.0371 m/s. When increasing the inlet velocity of water, a larger pressure drop was observed. Simulation of heat transfer on a single row, single cooling channel design of a battery pack was performed with a channel velocity of 0.03 m/s, which imitates the 4-channel design under the heat generation produced at a charging rate of 0.75 C. An inlet temperature of 30 °C was used to keep the maximum temperature of the battery at 30.706 °C. The temperature difference over the battery pack was approximately 0.4 °C.*

**Keywords:** *Standard deviation, Channel counts, Liquid-cooling plate*

## 1. Introduction

At present, Electric vehicles (EVs) tend to be the solution for modern vehicles. EVs require fewer parts compared to Internal Combustion Engine Vehicles (ICEVs) and can use electricity from alternative energy resources such as wind turbines, photovoltaics, water dams, etc. However, battery pack cost, driving range, and thermal management systems are the challenges of EVs. Especially the thermal management system, which needs to be developed to prolong the life of the battery pack.

### *1.1 The Effect of Heat on Battery Performance*

The battery is one of the most important parts of electric vehicles (EVs). The modern development of EVs requires higher capacity and power densities from battery packs. It is always expected that the number of battery cells can be packed as much as possible to maximize the output capacity and power density. However, high power load usage leads to a serious thermal issue due to heat generation. The temperature is sensitive to the battery performance and lifetime of battery cells. If the battery temperature is higher, the battery performance is higher because the higher temperature can accelerate the chemical reaction over the rated limit as shown in Fig. 1.

* Corresponding author: J. Charoensuk
E-mail address: jarruwat.ch@kmitl.ac.th

On the other hand, the battery life is lower when the battery temperature is higher, as shown in Fig. 2, and the last point is that the optimal battery temperature needs to be less than 33oC to protect the battery life span. Therefore, a suitable battery temperature needs to be considered. Greco et al. [1] have reported that the battery temperature should be maintained in the range of 20-40ºC and the maximum temperature difference for entire packs should be less than 5ºC.

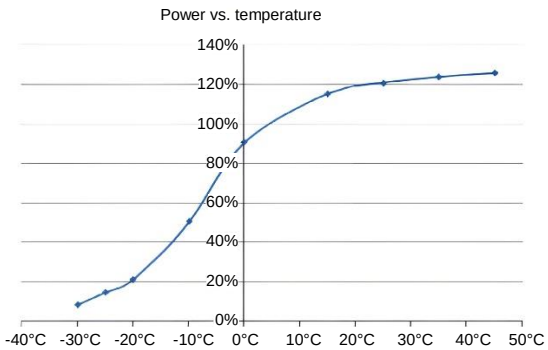


**Fig. 1.** The power as a function of the lithium-ion

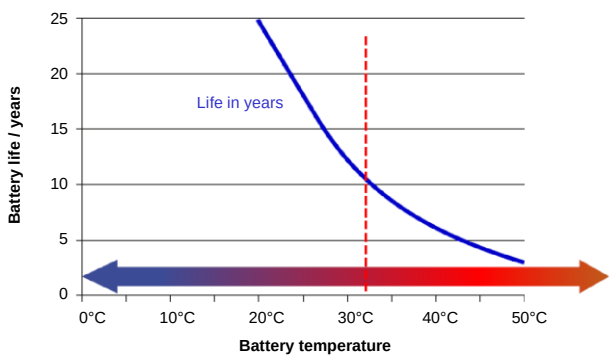


**Fig. 2.** The battery life of lithium-ion battery temperature

*1.2 Battery Cooling System*

There are different forms of thermal management for battery packs. They are primarily divided into three categories:

Firstly, using coolant in liquid form. Tesla utilized a dual-circuit liquid cooling system in a wavy tube placed between cylindrical cells, using a refrigerant circuit for all connections [2] to cool the liquid inside. Indirect liquid cooling is kept outside the enclosure to avoid leakage of the coolant, as some manufacturers use a cold plate between each prismatic cell that has several microchannels for convective heat removal from batteries. During the operation of the liquid cooling system, the heat would quickly transfer from the coolant to the cold side, as explained by Lyu et al. [3]. Next, [4, 5] explained that a U-shaped fluid channel was adopted and water was used as the coolant liquid flowing along the cooling channel attached with an aluminum block on both cold sides of the thermoelectric cooling plate. Compared with other fluids at the same flow rate, liquid cooling systems can be quite good at reducing a significant quantity of heat from the batteries. [6-8] explain that in terms of practical design and efficient cooling of Li-ion battery modules, they were primarily used in the cooling system. However, the liquid cooling system needs more attention because of liquid leaks and corrosion.

Secondly, using a phase-change material cooling system that can efficiently lower temperatures in the battery modules and reduce the temperature differences. This type also has limitations in terms of phase changes in volume and encapsulation.

Finally, the air-cooling system is easily available for cooling purposes inside low-density batteries [9]. For the passive cooling system, the Nissan Leaf simply used fresh air to cool the battery pack, and the exhaust air was emitted directly into the ambient air [10, 11], but it also had low capacity and low thermal conductivity when using different configurations of air flow rate and electric vehicles [12, 13]. Despite [14, 15], which used a cooling system inside the HVAC that maximized its efficiency by utilizing the vehicle's climate control system to heat, ventilate, and cool the vehicle, it was found that air cooling had the advantage of being simple to install and lightweight. However, [16] explained that air cooling had the disadvantage of poor cooling effectiveness and was insufficient to sustain temperatures under adverse circumstances. One of the limitations of assembling battery packs in an electric car is space. Consequently, the liquid cooling system has been chosen because it is more effective than the air-cooling system in terms of space [13, 17].

This research focuses on the NSTDA's patent-new design, and it was expected that the design would be better suited for battery heat management systems to use the liquid cooling method and water as the coolant. It has many advantages, as explained before. In this Investigation, There are one hundred eighty Li-ion battery cells in the battery pack. Five battery modules are packed within aluminum cooling plates, and each battery module has thirty-six cells, as shown in Fig. 3.

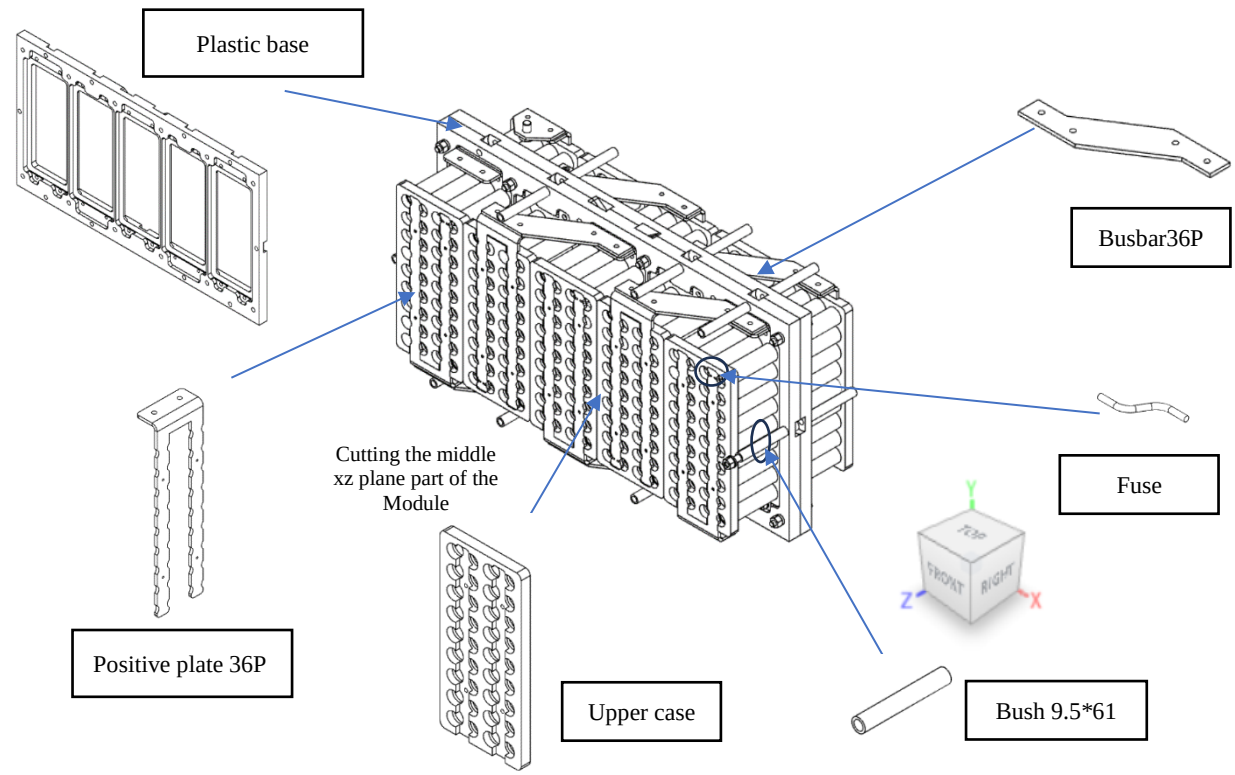


**Fig. 3.** 10S36P Battery Module Model

*1.3 The 10S36P Battery Module*

For simplicity in problem specification, while keeping the essential components for thermal analysis, the cooling pad and flow channel of a battery module was modeled. Following are the rationales of the problem specification.
1st step: Discard the upper case and positive plate because they are not considered for cooling in the positive terminal.
2nd step: Neglect the ohmic heating on the busbar that conducts the heat to the positive terminal. So, the bus bar will be removed.
3rd step: Discard all of the insulation parts [the bushes and all connectors] that can fasten the battery module.
4th step: Discard the plastic base because it is an insulation part and has lower thermal conductivity.
5th step: Using the x-z plane to show half the cooling module because the cooling system is symmetric. A submodule of the battery cooling system that contains the negative terminal plate, anodized aluminum plate, and nickel plate was found and the liquid cooling plate will be further investigated.

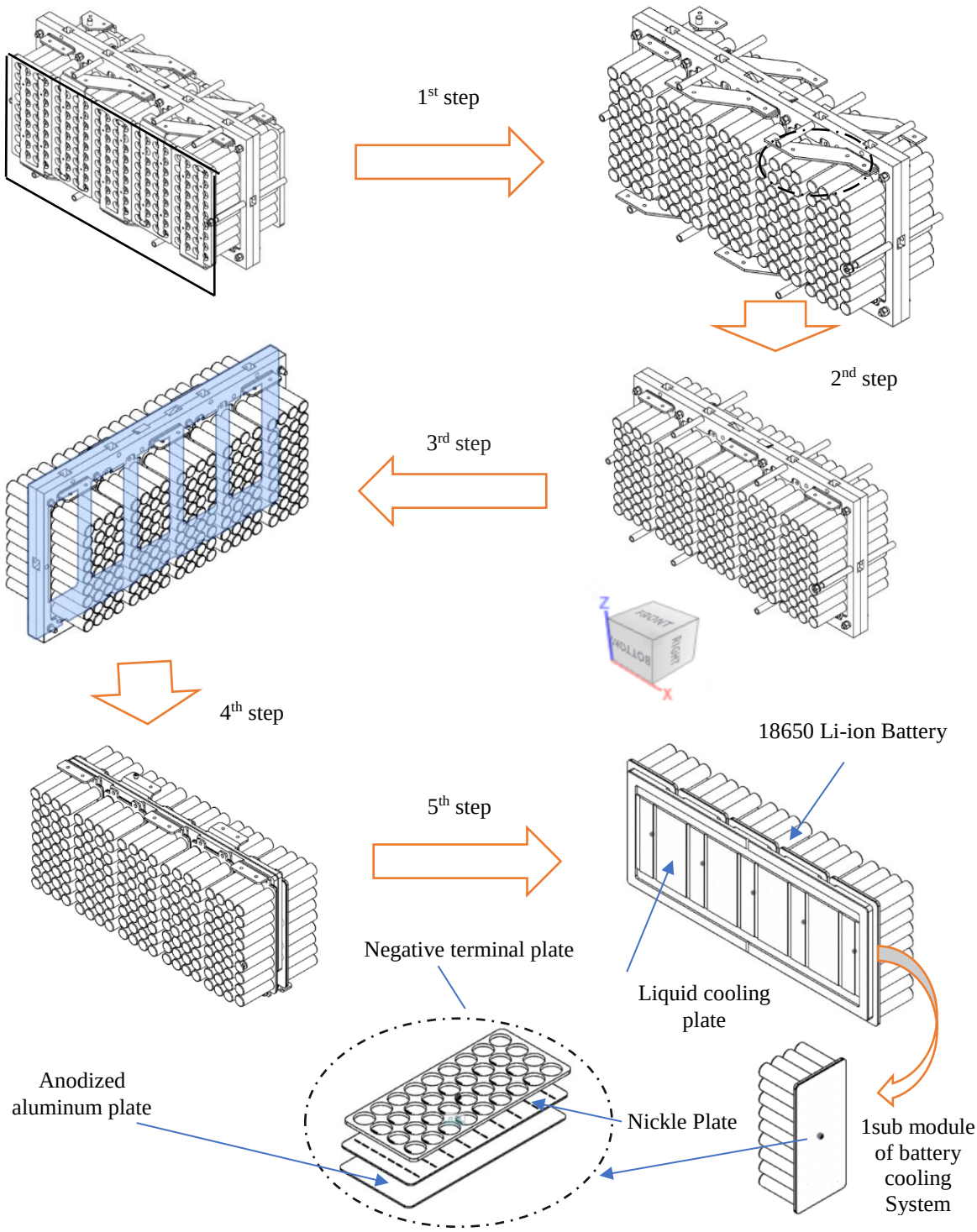


**Fig. 4.** 18650 Li-ion battery module with cooling channel configuration

Figure 4 displays the novel NSTDA battery module, which has one hundred and eighty 18650 Li-ion battery cells in the battery pack. Each battery module contains 36 cells and is enclosed within aluminum cooling plates. This module is made up of several parts. The first is the busbar, which is a copper strip with connectors for connecting to the battery's negative terminal and is intended to restrict potential negative differences and reduce multiple connections to specific terminals. Then, there is the plastic base, which acts as insulation between the battery pack on both sides.

When only each battery module is considered, it has three parts: the nickel coating, which contributes to higher energy density; a larger storage capacity and enhanced electrical conductivity. Anodized aluminum plate can create a stable aluminum oxide layer. This plate is used as a cooling liquid plate because it can protect the dielectric substrates from being damaged while the heat is transferred through the battery module.

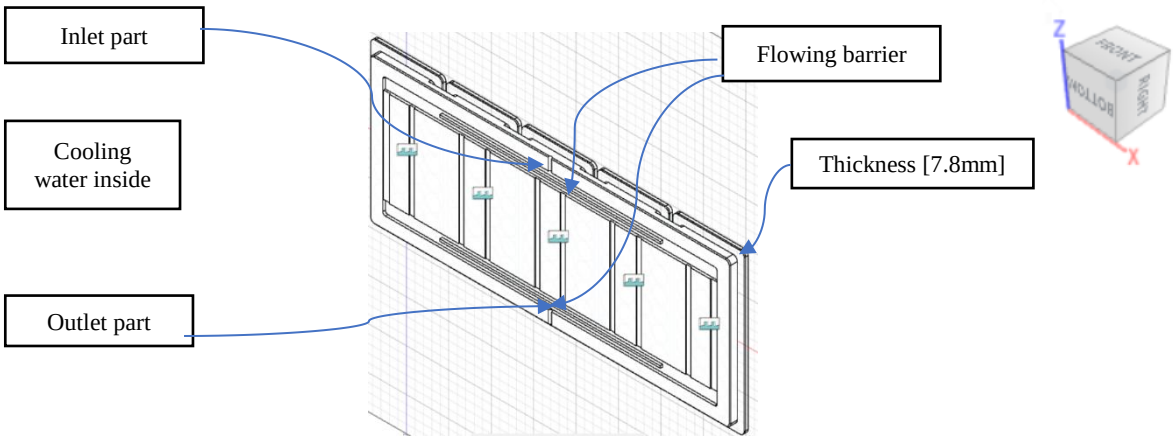


**Fig. 5.** Previous design of liquid cooling plates with two flow channel per base for the water-cooling system

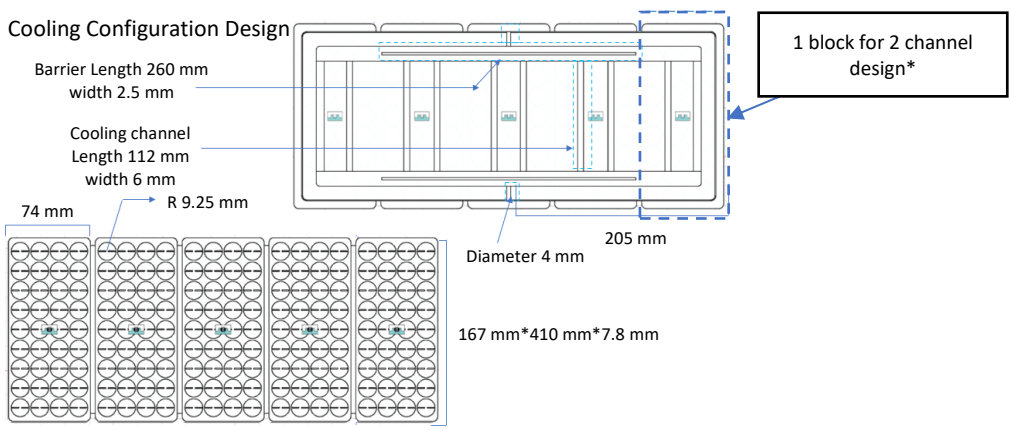


**Fig. 6.** Specification of previous design of liquid cooling plate

*1.4 Cooling Channel Specification*

The bottom plate's output side is where the liquid channel's outflow is located, as indicated in Fig. 5. The liquid path connects the cooling plate to the bottom plate, and the dimensions of the cooling channel are 167*410*7.8 mm in width, span, length, and thickness, respectively. Next, the cooling barrier dimension is 260*2.5mm. Water flows through a water channel 6 mm wide and 112 mm long. Finally, the liquid channel features a circular inlet and outlet of 4 mm in diameter as shown in Fig. 6.

This investigation focuses on factors affecting the performance of the liquid cooling plate, such as the pressure drop and temperature difference between inlet and outlet in the channel, by varying the number of cooling channels, the mass flow rate, and the inlet temperature of cooling water.

*1.4.1 Problem Simplification*

- Divide the aluminum cooling plate by half along the symmetry plane into 2.5 blocks of channels [length: 96.25 mm] and each block has 2, 3, 4, or 6 channels depending on each channel design. The cooling channel gap

was kept constant at 6 mm and 1 mm depth. This model was used for the simulation of flow in the cooling channel [steady state condition].

*1.4.2 The Modification of the Liquid Cooling Pad*

- Adjusted the distance between cooling channel blocks to be 41,32.5,20.5 and12 mm from center to center for 2,3,4 and 6 numbers of channels per base, respectively, as shown in Figures 7, 8, 9 and 10.
- Decreased cooling barrier length from 260 mm to 160 mm to improve water flow distribution in cooling channel configuration while the cooling gap length was fixed at 6 mm.

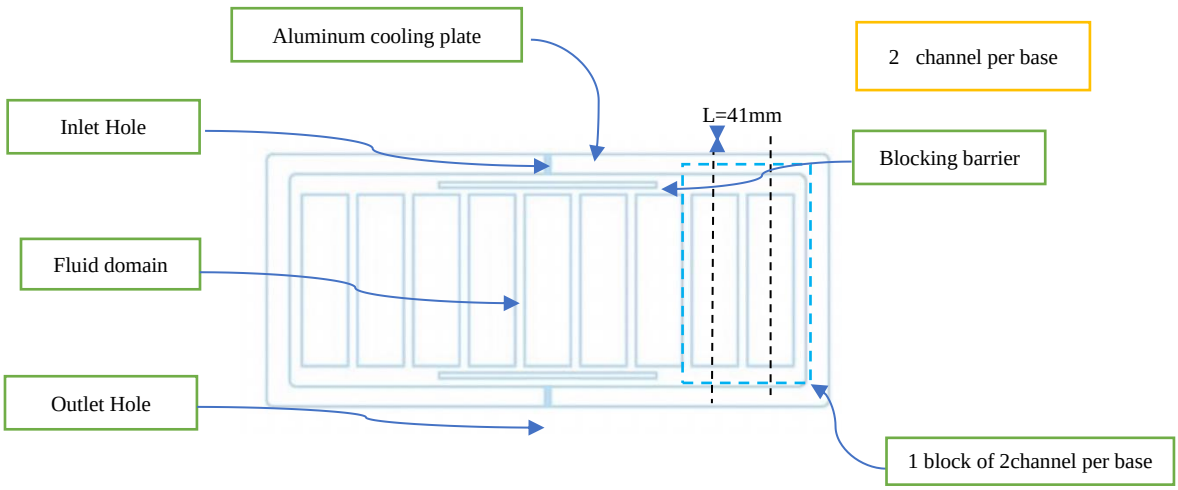


**Fig. 7.** Number of Cooling channels = 2*5=10

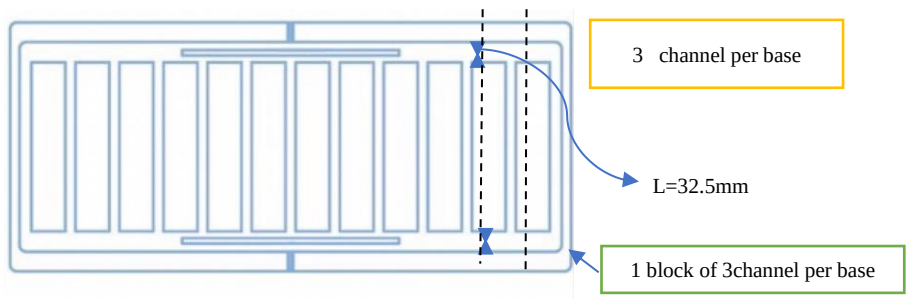


**Fig. 8.** Number of Cooling channels = 2*6=12

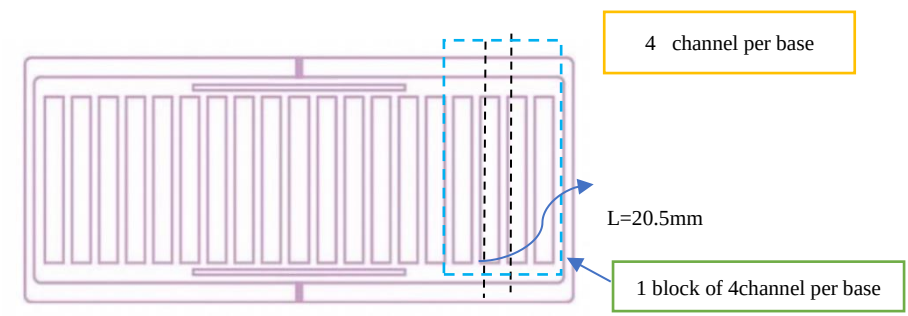


**Fig. 9.** Number of Cooling channels = 2*10=20

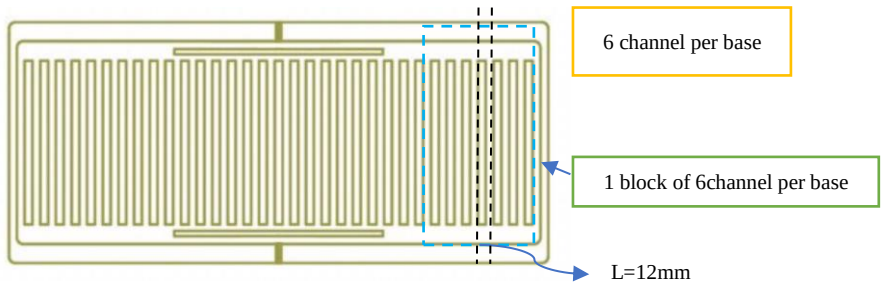


**Fig. 10.** Number of Cooling channels = 2*17=34

Figures 7, 8, 9, and 10 show the new design by varying the number of cooling channels inside the cooling plate that is located in the middle of the 10S36P battery module. The main variables used in this investigation were inlet temperature, inlet water velocity, and the number of cooling channels. The system's total cooling capacity from the cells can be impacted by the aforementioned variables. Moreover, the desirable differential temperature between battery packs should be less than 5°C, which is desirable for maximizing the utilization of the battery pack by considering the cooling plate design.

[18] illustrated more clearly that the temperature field of the unit composed of the liquid cooling plate and battery cell was analyzed under the conditions of an inlet temperature of 25°C at a charging rate of 0.75 C. For the final result, the temperature of the cooling tube of the liquid cooling plate increased gradually from inside to outside; the highest temperature was 31.2 °C, and the temperature difference was 6.21 °C. The target value of the temperature difference for our design should be within 5 °C.

Our simulation was also carried out with the heat generation of the battery at a charging rate of 0.75 C to evaluate the temperature difference, the pressure drop, and the heat removal rate.

## 2. The Parametric Study of the Cooling Channel

The battery thermophysical parameters and properties of the material are displayed in Table 1.

**Table 1:** Properties of Material

| Material | Phase | Thermal Conductivity [W/(m.K)] | Heat Capacity [J/(kg.K)] | Density [kg/m$^3$] | Heat Ratio | Viscosity [Pa.s] |
|---|---|---|---|---|---|---|
| Battery Cell | Solid* $[k_x, k_y, k_z]$ | {1.01, 30.22, 1.01} | 750 | 2690 | - | - |
| Aluminum | Solid | 155 | 893 | 2730 | - | - |
| Coolant | Liquid | 0.405 | 3300 | 1078 | 1 | 0.00429 |

*Refer to the global coordinates of the 10S36P battery module model received from Fig. 3.*

### *2.1 Heat Generation in the Battery Cooling System*

Although the heat generation rate varies with charging time, its maximum value was adopted as a constant, and the problem was simplified to be a steady state. This ensured that the simulated temperature of the battery would not exceed the instantaneous temperature during the charging period at a rate of 0.75 C.

### *2.2 The Cooling Strategy in Cooling Channel Simulation*

#### *2.2.1 Mass flow rate selection*

An investigation of the effect of the flow rate on cooling performance is carried out based on steady-state simulation. The flow speeds were simulated in the sequence of 50 L/h (0.5 m/s), 100 L/h (1.0 m/s), 200 L/h (2.0 m/s), and 300 L/h (3.0 m/s).The Reynolds number of water in channels and channel velocity would be investigated and compared at various numbers of cooling channels.

*2.2.2 Inlet Temperature Selection*

In this simulation, the battery was assumed to be under charging conditions with a constant current mode [SOC > 0.8] at a rate of 0.75 C. The simulation first used low water velocity at 0.5 m/s, and water temperatures started at 25 °C, followed by 30 °C, 35 °C, and 40°C, respectively.

*2.3 Governing equation of the water-cooling system*

Each battery is assumed to be identical, considering changes in geometry and chemical composition. The basic governing equations of fluid flow and heat transfer for cylindrical battery cells will be discussed below. To solve the 2D steady flow over battery cells, the continuity equation, momentum equation, and energy equations were written as follows:

Continuity equation

$$\nabla(\vec{v}) = 0 \tag{1}$$

Momentum conservation equation

$$\frac{\partial \vec{v}}{\partial t} + (\vec{v}\nabla)\vec{v} = -\frac{\nabla \rho}{\rho} + \frac{\mu}{\rho}\nabla^2\vec{v} \tag{2}$$

Where $\nabla$ = the divergence (the partial derivative)
$\vec{v}$ = the velocity vector of the cooling water
$\rho$ = the cooling water density =998 [kg/m$^3$]
$\frac{\partial \vec{v}}{\partial t}$ = the partial derivative of velocity vector change with time
μ = the dynamic viscosity coefficient of cooling water (Pa·s)

Energy conservation equation

$$\rho C_P \left(v_x \frac{\partial E}{\partial x} + v_y \frac{\partial E}{\partial y}\right) = k_T \left(\frac{\partial^2 E}{\partial x^2} + \frac{\partial^2 E}{\partial y^2}\right) \tag{3}$$

Where $\nabla$ = the divergence (the partial derivative)
$C_P$ = the specific heat capacity of cooling water= 4.187 [kJ/kg·K]
$v_x$ = the velocity of cooling water in x direction (m/s)
$v_y$ = the velocity of cooling water in y direction (m/s)
$\frac{\partial E}{\partial x}$ = the partial derivative of thermal energy per unit pathlength in x direction
$\frac{\partial E}{\partial y}$ = the partial derivative of thermal energy per unit pathlength in y direction
$k_T$ = the thermal conductivity (W/m·K)
E = the thermal energy (J)

*2.3.1 The Calculation of Heat Generation*

For the cooling system, the assumption used to calculate the heat generation of the battery cell that the temperature of the entire battery was constant, so the term for the battery's internal conductivity was left out, as was the heat transfer from the battery cell to an electrical wire and the surrounding environment. The equation below can be used to estimate heat generation [14, 19].

$$Q(t)_J + Q(t)_E = Q(t)_b \tag{4}$$

The heat generated inside the battery is denoted by the symbol $Q(t)_b$, which is composed of two sources: Joule heating and entropy change-related heat generation. The two sources of heat creation are specified in Equations (5) and (6) as

$$Q(t)_J = I^2 R_{int} \quad (5)$$

Where $Q_J$ stands for the heat of Ohmic losses, often known as Joule heating (W), I for battery current (A), and $R_{int}$ for internal resistance, which is made up of three terms: diffusion resistance, ion transport resistance, and Ohmic resistance [20].

$$Q(t)_E = -T\Delta S\frac{I}{nF} \quad (6)$$

Where $Q_E$ is the heat generation due to entropy change (W), $T$ is the absolute temperature of the battery (°C), $\Delta S$ is the entropy change (J/K), n is the number of electrons (mol) and $F$ is Faraday's constant ($9.65 \cdot 10^5$ s·A/mol).

Then, it is also possible to estimate the removal heat rate inside the battery cooling channel.

$$\text{Q}= \dot{q} =\dot{m}_w C_P(T_o - T_i)\ ; \quad \dot{m}_w = \rho_\omega \dot{v}_w \text{ A}= \pi(\tfrac{\text{D}}{2})^2;\ \dot{v}_w = \text{vA} \quad (7)$$

Where Q = the heat removal rate [kW]
$\dot{m}_w$ = the mass flowrate of inlet water [kg/s]
$\dot{v}_w$ = the volumetric flowrate of inlet water [$m^3$/s]
$\rho_\omega$ = the cooling water density=998 [kg/$m^3$]
$T_i$ = Inlet temperature [°C]
$T_o$ = Outlet temperature [°C]
v = Inlet velocity of cooling water [m/s]
A = Cross-sectional area [$m^2$]
D = Diameter of Inlet cooling Tap (m)

Finally, the battery state of charge (SOC)is estimated by ampere-hour integration.

$$SOC = SOC_{t=0} - \frac{1}{C_N}\int I(t)dt \quad (8)$$

where $SOC_{t=0}$=1 (when the battery is 100% charged)and $C_N$is the nominal capacity of the cell.

*2.4 Heat Generation Rate under Various Discharging Conditions*

Kulranut et al. [21] explained that the battery cell's thermal properties are evaluated during charging and discharging in the constant current (CC) and constant voltage (CV) modes. The current stays constant during the initial stages of charging in CC mode at around 80–90% of SOC when the battery is almost fully charged.

**Table 2:** Summary of maximum heat transferred rate, maximum temperature at various C-rate retrieved from Kulranut et al. [21]

| Event | Charge | | | Discharge | | |
|---|---|---|---|---|---|---|
| Current rate | 0.25C | 0.5C | 0.75C | $1^{st}$1C | $2^{nd}$1C | $3^{rd}$1C |
| Maximum heat transferred rate(W) | 0.073 | 0.145 | 0.307 | 0.953 | 1.022 | 1.041 |
| Maximum temperature (°C) | 36.361 | 41.709 | 45.813 | 51.813 | 52.462 | 53.012 |

*For the current investigation, the maximum temperature is selected at 0.75C during charging event*.

The commercial 18650 lithium-ion cells from the Toriyama brand with a Li-Ni-Mn-Co (NMC) cathode were used in this investigation. At a charging rate of 0.80 C, the battery is 80% charged and gains the maximum charging current [2A]. After this point, the voltage of the battery would continue to decrease in CV mode, as received from Kulranut et al. [21]. Based on experimental results (Table 2), focusing only on the charging process, the maximum temperature at the battery surface was found at a charging rate of 0.75 C; however, we are not considering the heat value at the discharge rate because it is an intermittent rate and normally takes a short period of time. Finally, the heat generation rate will be decreased to zero at the end of the discharge process.

*2.5 The Behavior of the Volumetric for Heat Generation Rate*

Table 3 shows the average heat generation and the percentage of variation when using different current charging rates [0.5C, 1C, and 1.5C].

**Table 3:** Maximum heat generation rate retrieved from Paccha-Herrera et al. [15]

| C-rate at charging Process | Volumetric heat generation rate (W/m3) | Percentage of Variation (%) |
|---|---|---|
| 0.5C | 5761 | 30.9 |
| 1C | 23588 | 5.8 |
| 1.5C | 52715 | 0.5 |

From Table 3, it is necessary to interpolate between 0.5C and 1C to find the maximum heat generation rate (w/m3) at 0.75C, which is between 14674.5 $W/m3$ and 15000 $W/m3$.The maximum percentage of variation of 30.9% at 0.5 C and 0.5% at 1.5 C, but the ideal range is between 7% and 14% retrieved from Paccha-Herrera et al. [15].

## 3. The Numerical Analysis of Battery Module

The model was made by CAD Software for setting boundary conditions, meshing part, and solver setting. After that, the steady-state model of the cooling channel will be used to find the temperature at outlet, pressure at outlet, and water velocity inside channel by varying parameters [inlet temperature, inlet velocity, and the number of cooling channels].

*3.1 Geometry and Materials*

The 3D-model CAD file used in this work includes solid and fluid elements. The 36 battery cells in the battery module, 1 nickel plate, 1 insulation layer, and 1 anodized aluminum plate, make up the work's solid components.

*3.2 Computational Domain*

The geometry of the battery module based on the cooling method reduced the complexity of the previous model. It meant that a few parts of the battery module were not considered, such as the insulator between battery cells, small aluminum conducting wires (fuses), the positive and negative busbars, and the plastic housing plate, because a little heat can be transferred to these parts. Secondly, the battery model was performed using steady-state models to investigate the maximum temperature of battery cells. Hence, the fluid flow was taken as laminar with non-isothermal flow. Finally, the simplified geometry of the battery cell with a fluid domain was used to study the thermal characteristics of the battery cell. However, in order to reduce the computational time due to the large number of mesh elements, the half-symmetric cooling model was used, as shown in Fig. 11.

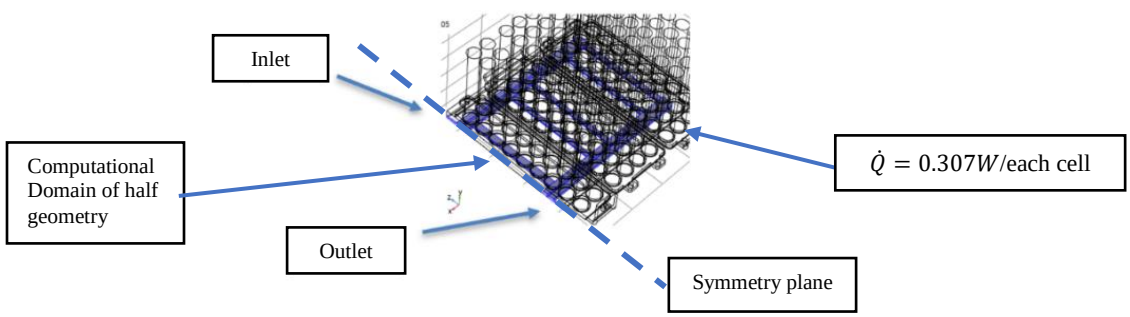


**Fig. 11.** The geometry of the cooling channel with coolant liquid inside

*3.3 Setting Boundary Condition in Steady State Model*

From Table 4, all cases of simulation are $4^3$ or 64. Selections of some cases were made that yielded the best cooling parameters, such as the maximum temperature of the battery being the least ($T_{b,min}$) with the minimum pressure drop. For a steady state result, selection was also made for cases with inlet velocity and inlet temperature of two-channel, three-channel, four-channel, and six-channel designs with a constant heat source, then showing the result of flow parameters and the maximum temperature of the battery to see the cooling performance among all designs.

**Table 4:** The Steady-state input - output parameters

| **Parameter1** **V_inlet (m/s)** | **Parameter2** **T_inlet of coolant water (°C)** | **Parameter3** **Number of Channels** |
|---|---|---|
| 0.5 | 25 | 2 |
| 1.0 | 30 | 3 |
| 2.0 | 35 | 4 |
| 3.0 | 40 | 6 |

*3.4 The Mesh Generation of Cooling Channel Model*

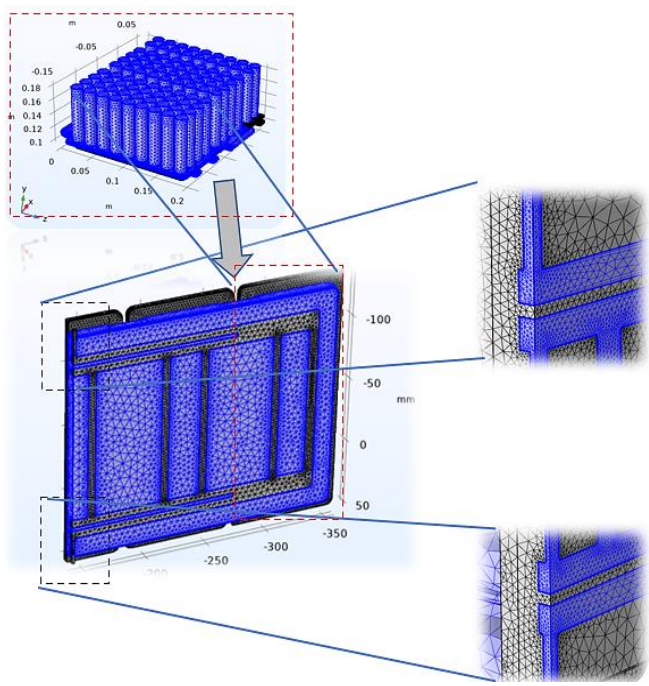


**Fig. 12.** The mesh generation on the cooling channel with the 18650 Li-ion battery module

The division of multizone in the mesh description was shown in Fig. 12. A meshing part has been set up for the fluid area to provide simulation quality. The standard size was around 0.25 mm. As a general rule, when volume meshing is initiated, the base size refers to the size of the largest elements in the fluid domain. If the base size was large, the mesh would be coarser, whereas if the base size was small, the mesh would be finer. The simulation of the battery was performed with different mesh sizes until insignificance change was observed and after the number of grids reached $8*10^5$, the calculating results did not significantly change with the variation of the meshes. The essential feature of the independence mesh statistics was displayed below in Table 5.

**Table 5:** The mesh statistics inside mesh model

| Description | Value |
|---|---|
| Average element quality | 0.6574 |
| Tetrahedron | 670752 |
| Pyramid | 514 |
| Prism | 21018 |
| Triangle | 208732 |
| Quad | 2664 |
| Edge element | 23704 |
| Vertex element | 1107 |

*3.5 Setting Heat Generation as Boundary Condition*

For 18650 Li-ion battery, the radius of the battery is 9 mm and h = 65 mm.

Under a charging rate of 0.75 C, the maximum heat generation per unit cell was [0.307 W], and the entire volume of 18650 Li-ion battery cell was $1.6 * 10^{-5} m^3$ then the maximum heat generation rate was set at $\frac{0.307}{1.6*10^{-5}} = 19187.5\ W/m^3$ (see Fig. 13).

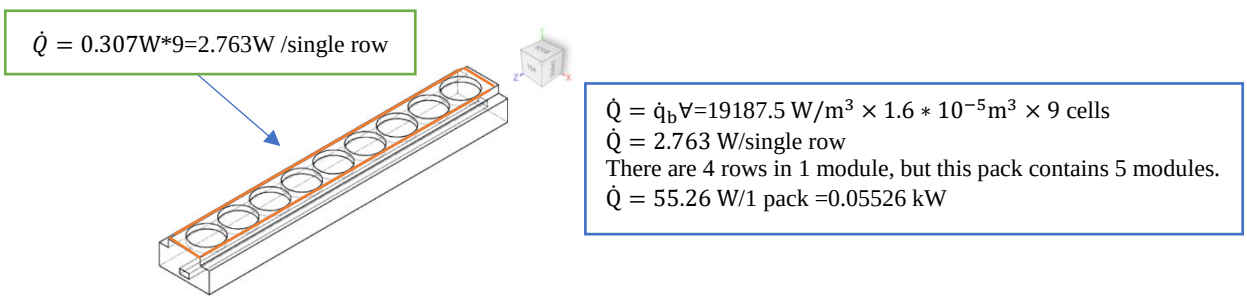


**Fig. 13.** Setting heat generation inside the simplified battery model

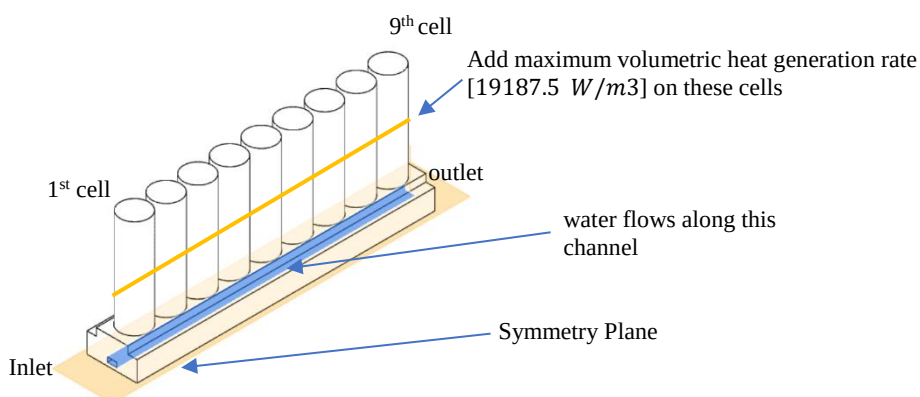


**Fig. 14.** The simplification battery model assessment

The simplified battery model (see Fig. 14) was used to reduce the time consumption of parametric studies by considering the steady flow inside the cooling channel and estimating the maximum temperature of the battery pack from the 1st cell to the 9th cell using steady-state simulation.

## 4. Results and Discussion

### *4.1 Temperature Difference and Pressure Drop Plot with an Inlet Velocity of Cooling Water*

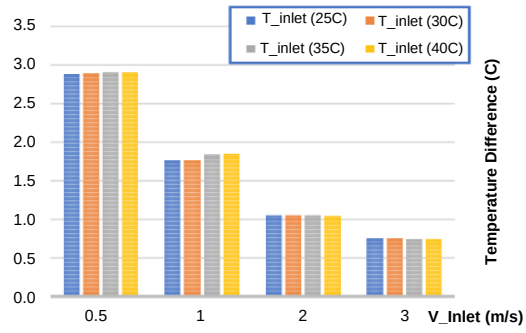


**Fig. 15.** Result of temperature difference compared with inlet velocity started with inlet temperature: 25°C to 40°C

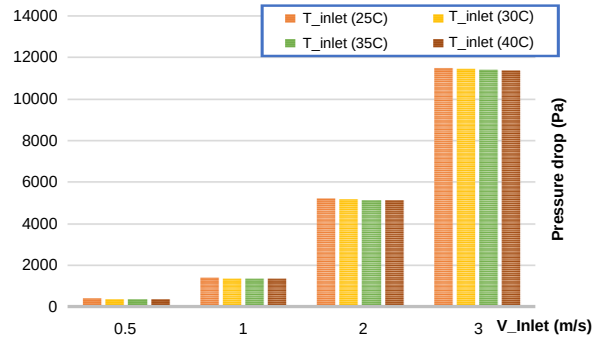


**Fig. 16.** Result of pressure drop compared with inlet velocity started with inlet temperature: 25 ºC to 40 ºC

According to Figs. 15 and 16, increasing inlet water velocity caused the water temperature difference between the inlet and outlet sides to be lower. A higher amount of water in the inlet caused a significant increase in pressure drop; however, when using a small amount of inlet velocity, the pressure of water inside the cooling channel was observed to be the lowest, with a slight effect at inlet velocity 0.5 m/s due to the inlet temperatures of cooling water. Furthermore, the temperature difference increased to approximately 3°C.

A high-water flow rate creates a high pressure drop, reaching its maximum at 12000 Pa when utilizing the maximum inlet water flow rate of 3 m/s. The water flow rate has a significant impact on the pressure drop and the temperature difference.

Finally, the results of temperature difference and pressure drop have not changed much when increasing the inlet temperatures of water, but these values have been greatly affected when the inlet velocity is increasing, as used in the boundary conditions.

### *4.2 Energy Conservation among Different Numbers of Channels [2, 3, 4, and 6 Channels per Base]*

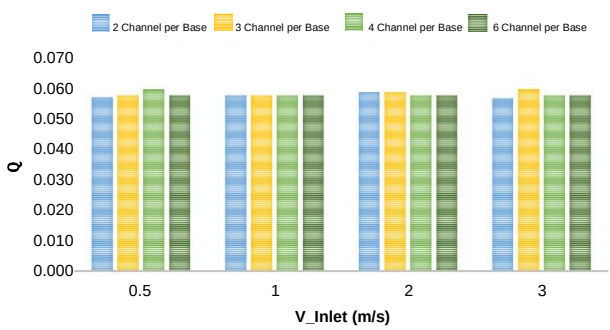


**Fig. 17.** Inlet Temperature 25°C

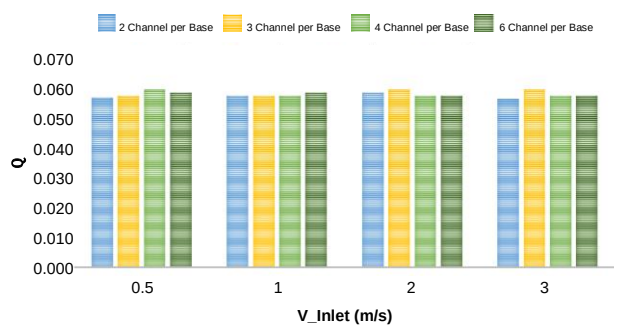


**Fig. 18.** Inlet Temperature 30°C

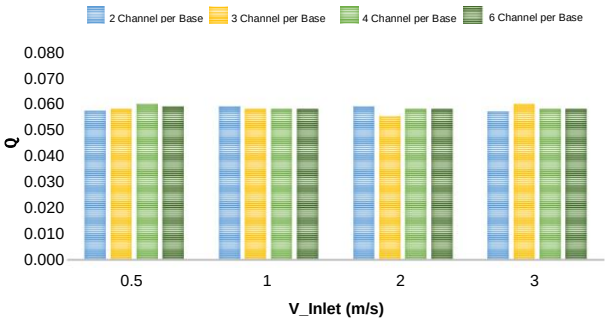


**Fig. 19.** Inlet Temperature 35°C

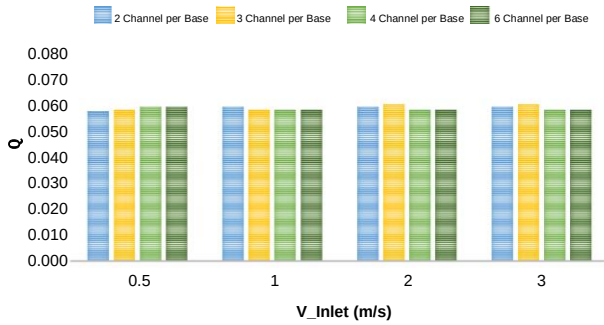


**Fig. 20.** Inlet Temperature 40°C

Figures 17, 18, 19 and 20 display the steady-state results of the heat removal rate (kW) using various numbers of cooling channels [2, 3, 4, and 6 channels per base] with the starting water velocity [0.5, 1, 2, and 3 m/s] and inlet temperature [25°C, 30°C, 35°C, and 40 °C]. The heat removal rate that occurred inside the battery was consistent at 0.059 kW, as proven by the principal theory of the steady flow energy equation. According to Fig. 18, when applying an inlet temperature of 30°C with an inlet velocity of 2 and 3 m/s, it had a little error of just 5.8% at a heat removal rate of 0.0605 kW.

The precise value of heat removal rate ($\dot{q}$) obtained from eq. (7) was 0.0553 kW, which was very close to the simulation results that had previously been explained.

To sum up, all simulation results express the result as being consistent with a minimal numerical error using various designs of cooling channels, no matter how much inlet velocity and inlet temperature of water were used.

*4.3 The Comparison of the Standard Deviation of Channel Velocity with Various Numbers of Cooling Channels*

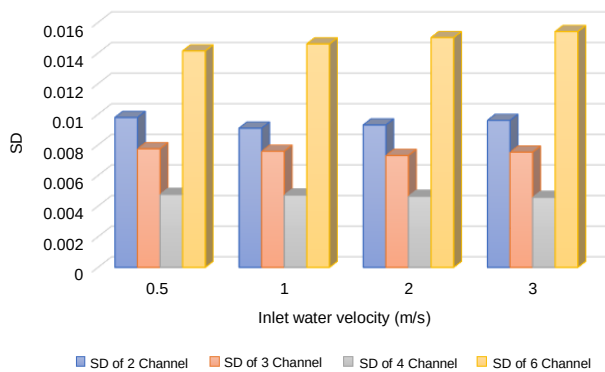


**Fig. 21.** The Standard deviation with inlet velocity of water (m/s) using different numbers of cooling channels

The cooling barrier length was 260 mm for the previous cooling block version. When using an inlet velocity of 0.5 m/s and an inlet temperature of 30 °C, It was seen that 4-channel designs offer the most uniform flow distribution because the standard deviation was lowest at 0.0046, followed by 3-channel, 2-channel, and 6-channel designs, respectively, as seen in Fig. 21.

With an inlet velocity of 0.5 m/s and an inlet temperature of 30 °C, was setting boundary conditions. The maximum channel velocity in a 4-channel configuration was 0.042 m/s, the lowest channel velocity was around 0.031 m/s, and the average channel velocity was 0.037 m/s. Moreover, in a 3-channel design, the maximum was at 0.065 m/s, which was higher than 4-channels at 0.023 m/s [35.38%] when using the same inlet condition, as shown in Fig. 22.

*4.4 The Comparison of the Standard Deviation of Channel Velocity with Various Numbers of Cooling Channels [Reducing cooling barrier length]*

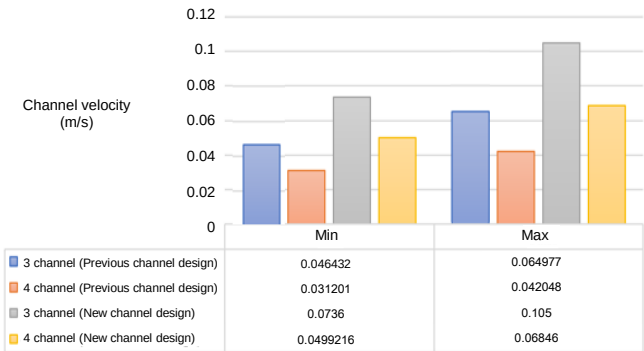


**Fig. 22.** The minimum and maximum of channel velocity when inlet velocity was 0.5 m/s compared with 3 and 4 channel designs

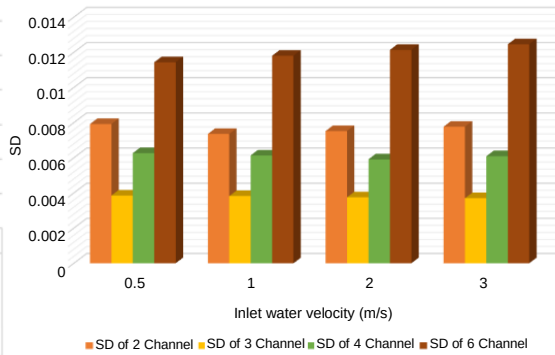


**Fig. 23.** The Standard deviation with inlet velocity of water (m/s) using different numbers of cooling channels

In addition to the above findings, the cooling barrier length was reduced from 260 mm to 160 mm to see its effect on water flow distribution in the cooling channel, while the cooling gap length remained constant at 6 mm.

For the modified version of the cooling block, the lowest value of the standard deviations was found in the 3-channel design at 0.0037 when the inlet velocity of cooling water was only 0.5 m/s, followed by the 4-channel, 2-channel, and 6-channel designs, respectively, which are all displayed in Fig. 22 and Fig. 23. After reducing the cooling barrier length, the standard deviation of all channel designs has decreased, which means the shorter length of the cooling barrier has a great effect on the dispersion of flow distribution. When increasing the inlet velocity of cooling water, the standard deviation remains stable, but it seems to increase slightly on a 6-channel design and reached its peak at over 0.012 when the inlet velocity of cooling water was 3 m/s.

Although the 3-channel design had the lowest standard deviation when using the modified version of the cooling block, the flow in the channel was less uniform due to a large velocity difference inside the cooling channel of 0.04 m/s. For the previous version of the cooling block, the 4-channel design reached only 0.026 m/s when using an inlet velocity of 0.5 m/s and had the lowest standard deviation, as stated in 4.3.

From the standard deviation and the channel velocity results that were both already compared, a 4-channel design performed the best uniformity of flow distribution because the least standard deviations brought the greatest velocity distribution, and the minimum channel velocity of this configuration was selected as the boundary condition in the simplified cooling model using steady state simulation.

*4.5 The Maximum Temperature of Battery in Steady-State Simulation*

The heat generation rate was approximately under a charging rate of 0.75C. Then this value was used as a constant heat source in the single-channel flow simulation. The results of channel velocity for four channels per base were revealed at $V_{avg}$ [0.037 m/s], $V_{max}$ [0.042 m/s], and $V_{min}$ [0.031 m/s] when use inlet velocity of 0.5 m/s. Finally, $V_{min}$ and the inlet temperature of the water at 30°C were selected as boundary conditions.

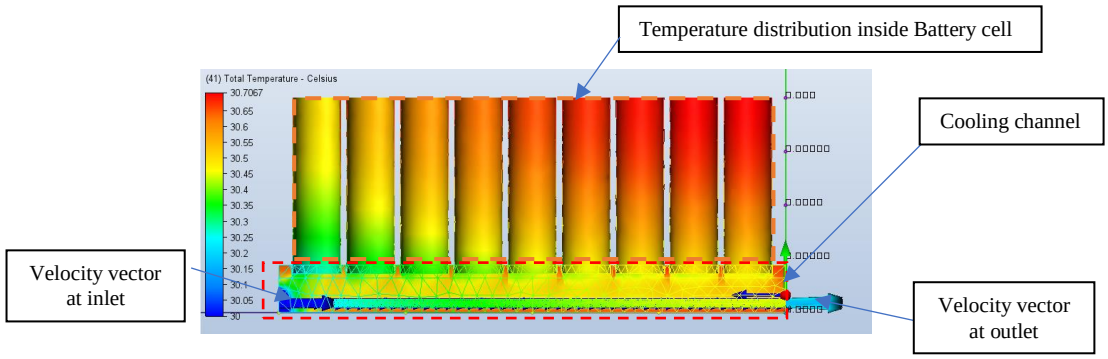


**Fig. 24.** The temperature contour of 9 battery cells under 0.75C charging rate

When the flow of water in the cooling channel ran through all nine batteries, the channel velocity at the outlet of the cooling channel followed the momentum conservation law. The temperature distribution inside a single row of the cooling channel increased from 30 °C [inlet zone] to nearly 30.5°C [outlet zone]. The result of the single flow simulation from the 1st cell to the 9th cell showed that under a 0.75 C charging rate in steady state, the greatest temperature of the battery was approximately 30.706 °C and yielded the highest percentage of battery performance [120%] from Fig. 1 using the inlet temperature at 30 °C, and the maximum temperature difference of the battery was 0.706°C (see Fig. 24).

In summary, after adjusting the coolant temperature, the battery temperature rises irrespective of the value of the inlet velocity. However, it can be stated that as the flow speed increases, the maximum temperature of the battery module will decline. Ohmic loss also caused rises in the battery temperature, while the heat was absorbed by the coolant through heat transfer, which resulted in a temperature difference in the battery.

To find the maximum temperature, the coolant inlet temperature was chosen to be less than 30°C. Battery life is the most important factor that influences battery aging and causes premature battery failure. Higher temperatures mean a faster chemical reaction inside the battery. The maximum temperature of the battery was found to be less than 33°C (see Fig. 2), so that battery life could be more than 10 years.

## 5. Conclusion

### *5.1 The Summary of Steady State Simulation*

- A 4-channel design offered the highest velocity uniformity of the water flow distribution among all channel configurations.
- The ability to remove heat from the battery when the inlet velocity increased from 0.5 m/s to 3 m/s was consistent at 0.0585 kW. When using an inlet temperature of 30°C with an inlet velocity of 2 and 3 m/s, it had a slight error of only 5.8% at a heat removal rate of 0.0605 kW.
- All cooling designs can produce very good water distribution when using low inlet velocities. However, when increasing the inlet velocity, the distribution of water in the channel got worse, especially for the 6-channel design, which had the highest standard deviation.

### *5.2 The Heat Generation Results in a Single Channel in The Battery Pack [9 Cells].*

- The highest average temperature at the 9th cell was 30.706 °C, which was lower than the maximum allowable battery temperature of 33 °C when using a channel velocity of 0.03 m/s with an inlet temperature of 30 °C as the boundary conditions.
- When the inlet water velocity ≥ 2.0 m/s, the flow became fully turbulent [Re = 6728.72], which was greater than the limited value of the laminar zone [Re<4000].The flow dispersion would be enhanced if the incompressible flow was steady. Moreover, discussing the same inlet velocity condition, the minimum channel velocity in a 4-channel [most uniform design] was 0.078 m/s [Re = 292.32], which was in the laminar zone.

- The inlet temperature should be less than or equal to 30°C to keep the maximum temperature at 33 °C [the maximum allowable battery temperature limit].

**Nomenclature**

| | |
|---|---|
| $R_{int}$ | Internal Resistance of battery (Ω) |
| $Q_J$ | Joule heating (W) |
| I | Battery current (A) |
| $Q_E$ | Heat generation due to entropy change (W) |
| T | Absolute temperature of the battery (°C) |
| $T_{max}$ | Maximum Surface temperature (°C) |
| $T_{avg}$ | Average temperature (°C) |
| $T_i$ | Inlet temperature of cooling water [°C] |
| $T_o$ | Outlet temperature of cooling water [°C] |
| Δs | Entropy change [J/°C] |
| ΔT | Temperature difference [°C] |
| ΔP | Pressure drop [Pa] |
| SOC | State of Charge |
| $P_{fluid}$ | Pressure of fluid in the cooling channel (Pa) |
| $V_{avg}$ | Average value for channel velocity of cooling water (m/s) |
| $V_{min}$ | Minimum value for channel velocity of cooling water (m/s) |
| $V_{max}$ | Maximum value for channel velocity of cooling water (m/s) |
| $C_p$ | Specific heat capacity of cooling water (J/kg·°C) |
| k | Thermal conductivity (W/m·°C) |
| Q | Heat removal rate (KW) |
| $\dot{m}_w$ | The mass flowrate of inlet water [kg/s] |
| $\dot{v}_w$ | The volumetric flowrate of inlet water [$m^3$/s] |
| $\rho_\omega$ | Density of cooling water [$Kg/m^3$] |
| A | Cross-sectional area of Inlet cooling Tap [$m^2$] |
| D | Diameter of inlet cooling Tap (m) |
| $\rho_{al}$ | Density of aluminum[$Kg/m^3$] |
| μ | Dynamic viscosity coefficient (Pa·s) |

**References**


[1] Greco A, Jiang X, Cao D. An investigation of lithium-ion battery thermal management using paraffin/porous-graphite-matrix composite. J Power Sources. 2015;278:50-68.

[2] Azizi Y, Sadrameli SM. Thermal management of a LiFePO4 battery pack at high-temperature environment using a composite of phase change materials and aluminum wire mesh plates. Energy Convers Manag. 2016;128:294-302.

[3] Lyu Y, Siddique ARM, Majid SH, Biglarbegian M, Gadsden SA, Mahmud S. Electric vehicle battery thermal management system with thermoelectric cooling. Energy Rep. 2019;5:822-827.

[4] Chantheve P, Hirai S, Lailuck V, Laoonual Y, Sriam P, Rompho S, et al. A simplified approach for heat generation due to entropy change in cylindrical LCO Battery. 2018 IEEE Transportation Electrification Conference and Expo, Asia-Pacific; 2018 Jun 6-9; Bangkok, Thailand. USA: IEEE; 2018. p. 1-5.

[5] Huang Y, Mei P, Lu Y, Huang R, Yu X, Chen Z, et al. A novel approach for Lithium-ion battery thermal management with streamline shape mini channel cooling plates. Appl Therm Eng. 2019;157:113623.

[6] Qian Z, Li Y, Rao Z. Thermal performance of lithium-ion battery thermal management system by using mini-channel cooling. Energy Convers Manag. 2016;126:622-631.

[7] Lan C, Xu J, Qiao Y, Ma Y. Thermal management for high power lithium-ion battery by mini channel aluminum tubes. Appl Therm Eng. 2016;101:284-292.

[8] Yang XH, Tan SC, Liu J. Thermal management of Li-ion battery with liquid metal. Energy Convers Manag. 2016;117:577-585.

[9] Saw LH, Ye Y, Tay AAO, Chong WT, Kuan SH, Yew MC. Computational fluid dynamic and thermal analysis of Lithium-ion battery pack with air cooling. Appl Energy. 2016;177:783-792.

[10] Alipanah M, Li X. Numerical studies of lithium-ion battery thermal management systems using phase change materials and metal foams. Int J Heat Mass Transf. 2016;102:1159-1168.
[11] Yan J, Wang Q, Li K, Sun J. Numerical study on the thermal performance of a composite board in battery thermal management system. Appl Therm Eng. 2016;106:131-140.
[12] Wang H, Xu W, Ma L. Actively controlled thermal management of prismatic Li-ion cells under elevated temperatures. Int J Heat Mass Transf. 2016;102:315-322.
[13] Lu Z, Meng XZ, Wei LC, Hu WY, Zhang LY, Jin LW. Thermal Management of densely packed EV battery with forced air-cooling strategies. Energy Procedia. 2016;88:682-688.
[14] Bernardi D, Pawlikowski E, Newman J. A general energy balance for battery systems. J Electrochem Soc. 1985;132:5-12.
[15] Paccha-Herrera E, Calderón-Muñoz WR, Orchard M, Jaramillo F, Medjaher K. Thermal modeling approaches for a LiCoO2 lithium-ion battery—a comparative study with experimental validation. Batteries. 2020;6(3):40.
[16] Chen D, Jiang J, Kim GH, Yang C, Pesaran A. Comparison of different cooling methods for lithium-ion battery cells. Appl Therm Eng. 2016;94:846-854.
[17] Ho VT, Chang K, Lee SW, Kim SH. Transient thermal analysis of a Li-ion battery module for electric cars based on various cooling fan arrangements. Energies. 2020;13(9):2387.
[18] Xu X, Li W, Xu B, Qin J. Numerical study on a water-cooling system for prismatic LiFePO4 batteries at abused operating conditions. Appl Energy. 2019;250:404-412.
[19] Barbir F. PEM fuel cells. In: Barbir F, editor. PEM Fuel Cells: Theory and Practice. Amsterdam: Elsevier; 2005. p. 33-72.
[20] Incropera FP, DeWitt DP. Introduction to heat transfer. 2nd ed. Hoboken: Wiley; 1990.
[21] Kulranut J, Depaiwa N, Yenwichai T, Intano W, Masomtob M. Improvement of estimation method for battery cell heat generation. J Res Appl Mech Eng. 2021;9(2):1-10.